

Performance of compressed nickel foam wicks for flat vertical heat pipes

Suggested abbreviated title: "Nickel foam wicks"

Geir Hansen^{a,*}, Erling Næss^a

^aDepartment of Energy and Process Engineering, Norwegian University of Science and Technology, Kolbjørn Hejes vei 1a, 7491 Trondheim, Norway

*Corresponding author:

E-mail: g.hansen@ntnu.no

Phone: +47 73593938

Fax: +47 73593580

Abstract

The fabrication and performance of wicks for vertical flat heat pipe applications produced by compression of nickel foams has been investigated. The permeabilities and the effective pore radii for the wicks were estimated from rate-of-rise experiments, using the model fluid heptane. The porosities of the wicks were measured using isopropanol. The results, which are new and of vital importance for optimum use of such wicks, show that the permeabilities and the effective pore radii are in the upper range for heat pipe use. The joining pressure required during the sintering of the wicks was determined, and it was discovered that the nickel foams turned hydrophilic during the sintering.

Keywords: Heat pipe, wick, nickel foam, sintering, rate-of-rise

Symbols:

| | | |
|-----------|----------------------------|---------|
| A_c | Wickcross sectional area | m^2 |
| g | Gravity constant (=9.81) | m/s^2 |
| H | Height | m |
| h_{fg} | Latent heat of evaporation | J/kg |
| m | Mass | kg |
| \dot{m} | Mass flow rate | kg/s |
| P | Pressure | Pa |

| | | |
|------------------|-----------------------|----------------|
| \dot{Q} | heat flow rate | W |
| r | Radius | m |
| r_{eff} | effective pore radius | m |
| t | Time | s |
| T | temperature | K, °C |
| V | volume | m ³ |
| W | Width | m |
| y | Height | m |

Greek symbols

| | | |
|---------------|-----------------------------------|-------------------|
| ε | Porosity | - |
| θ | Solid-liquid-vapour contact angle | Degrees (°) |
| κ | Permeability | m ² |
| μ | Dynamic viscosity | kg/(m·s) |
| ρ | Density | kg/m ³ |
| σ | Surface tension | N/m |
| δ | Thickness | m |
| Δ | Difference | |

Subscripts

| | |
|------|-------------------------|
| cap | Capillary |
| eff | Effective (pore radius) |
| evap | Evaporation |
| fric | Friction |
| g | Gravity |
| hs | Hydrostatic |
| l | Liquid |
| v | Vapour |
| 0 | Uncompressed |

1. Introduction

Well designed heat pipes have the ability to transport heat at high rates and at minimal temperature drop. The main reason for their high effectiveness is that the heat internally in the heat pipe is transported by vapour, utilizing evaporation and condensation of a working fluid. Heat pipes are in use in many fields and at many temperature levels, from cryogenic applications to the high temperatures in the metallurgical industries [1-2]. The number of available working fluids, especially for operation in the extreme temperatures, is limited. The same is true for the number of compatible construction materials and wicks. Inside the heat pipe the condensate is transported to, and distributed over the evaporator section by capillary forces created by a porous wick structure. The most attractive wick provides a high capillary pressure and at the same time an acceptable flow resistance. The heat pipe for a specific application is unfortunately often selected from a quite limited selection of heat pipe container materials, wick materials and structures, and working fluids. This is especially true for heat pipes needed for the extreme working temperatures. The current study was undertaken to provide wick design data for the wick of a vertical flat hybrid heat pipe/thermosyphon with potassium as working fluid, for operation up to 650°C in the metallurgical industry. Model fluids (heptane and isopropanol) were used to characterize the wicks, as the characterization experiments would be very difficult to carry out with potassium due to its reactivity with air and moisture. Overviews over established materials, structures and working fluids suitable for different working temperatures are available in textbooks [1-4]. Recently Dillig et al. [5] carried out experiments with planar heat pipes using sodium as working fluid and different types of wick structures (screen mesh, sintered plates and grooves). The capillary limitation was identified as one of the main challenges in their study, underlining the importance of the wick structure optimization.

Wick optimization and development are also given much attention by researchers working on lower temperature systems, particularly wicks of grooves and/or sintered powders for loop heat pipe applications in the computer industry [6]. Usually the goal is to achieve high capillary pressure and high permeability, but the weight of the wick structure can also be a parameter for optimization [7]. For conventional single phase cooling systems various methods of surface optimization exist [8-9], however, the present paper deals with experimentally obtained characteristics of compressed nickel foam which may in the future lend itself to similar optimization.

Wick technologies can be combined. Recently Li et al. [10] analysed the performance of a cylindrical heat pipe with a composite wick having high permeability axial grooves which were covered (but not filled) by a layer of sintered copper powder. The performance was compared to the performance of a heat pipe with larger grooves filled with copper powder. The heat pipe with the active grooves had lower total thermal resistance, but the same maximum heat transfer rate as the heat pipe without active grooves. Jiang et al. [11] successfully developed and tested a novel porous crack composite wick for microchip cooling for working temperatures below 60°C. Solomon et al. [12] used nanoparticles of copper to coat screen type wicks, and found that this reduced the thermal resistance in the evaporator of the heat pipe but increased the resistance of the condenser. The overall result was positive, since the total resistance was reduced.

Compression of nickel foam, as described by Sheehan et al. [13] and Queheillalt et al. [14], is one method of producing wicks which has so far not been given much attention. The method is particularly interesting because the degree of compression, and thereby the pore size and the wick properties can be tailored to best fit the requirement of the application at hand. Recently Silk and Myre [15] used compression to obtain the desired pore size for a carbon wick structure, for loop heat pipes using water as working fluid. Several layers of compressed foam can be sintered together to increase the total capacity of the wick. Huang, Franchi and Cai [16] created bimodal nickel wicks for heat pipes by sintering filamentary nickel powder onto uncompressed nickel foam. In the future even more tailor made wicks are anticipated, e.g. by sintering nickel powder onto compressed nickel foam.

Nickel foam was chosen as wick material by Queheillalt et al. [14] because it was considered compatible for a heat pipe using water as working fluid. Material compatibility makes nickel equally relevant for high temperature heat pipes using alkali metals such as potassium or sodium as working fluids. Stainless steel 304 is also compatible with potassium and sodium [1], but has a much lower thermal conductivity than nickel. Nickel foams are currently produced for the battery industry in large batches according to customer specifications. Unmodified foams usually have pore sizes of a few hundred microns, which are too large for heat pipe wick applications. The foams are usually characterized by the density, pore size and thickness. For heat pipe wick applications additional data are needed, especially related to the wettability and the flow characteristics of different wick and working fluid combinations. The key parameters for the flow characteristics are the permeability and the effective pore radius of the wick. The effective pore radius depends on the wettability, commonly described by the contact angle [17]. The porosity of the wick is another important parameter which is required in design processes, for instance in order to precisely calculate the amount of working fluid required in the heat pipe. In the present work the following elements have been investigated for the compressed nickel foam wicks:

- The wettability with water before and after the oxide reduction process.
- The joining pressure required on the layers during the sintering to achieve a mechanically strong multilayer wick.
- Porosities at different wick compression.
- Contact angles with heptane, estimated from measurements of maximum capillary rise and evaporation rates from the wicks.
- Effective pore radius and permeability estimates from rate-of-rise experiments with heptane.
- The effect of heptane evaporation and experiment duration on the rate-of-rise experiment results.
- The heat transfer capacity with potassium as working fluid.

2. Theory

In most heat pipe design calculations the wick is characterized by its porosity, permeability and effective pore radius. The theories behind the experimental determination of these parameters are based on assumptions which are mentioned in conjunction with the specific equations, however two recurring assumptions are:

- A capillary tube model is used to represent the wick.
- The density of the liquid phase is large compared to the density of the vapour phase, hence the vapour density can be neglected.

The permeability, κ , characterizes the frictional pressure drop characteristics of the liquid flowing in the wick as shown by Eq. (1) [18].

$$\frac{dP_{fric}}{dy} = -\frac{\dot{m}\mu}{\kappa A_c \rho} \quad (1)$$

where y is defined as positive in the upwards direction from the liquid bath level. This flow direction may also be called the vertical in-plane direction, and it is perpendicular to the “through thickness” flow direction as studied by Sheehan at al. [13].

If uniform evaporation is assumed over the wetted wick height, H , (as is the case for most heat pipes), Eq. (1) can be integrated to yield the total frictional pressure drop:

$$\Delta P_{fric} = -\frac{\mu_l}{\kappa \rho_l A_c} \dot{m}_{max} \left(\frac{H}{2} \right) \quad (2)$$

where \dot{m}_{max} is the mass flow rate at the fluid entrance end of the wick.

For vertical wicks there is also a hydrostatic pressure drop created by the liquid column in the wick [18]:

$$\Delta P_{hs} = -\frac{g \dot{m}_l}{\varepsilon A_c} = -\rho_l \cdot g \cdot H \quad (3)$$

The “pumping” pressure balancing the pressure drops is the capillary pressure. According to Eq. (4), which was derived from an ideal circular capillary tube, the influence of the contact angle (θ) is merged into the effective pore radius [18]. The capillary pressure becomes:

$$\Delta P_{cap} = \frac{2\sigma \cos(\theta)}{r} = \frac{2\sigma}{r_{eff}} \quad (4)$$

If the effective pore radius is determined from an experiment using a model fluid, the effective pore radius with the actual working fluid can be calculated from Eq. (5), provided that the contact angles of the respective fluids on the wick surface are known:

$$\frac{r_{eff,fluid1}}{r_{eff,fluid2}} = \frac{\cos \theta_{fluid2}}{\cos \theta_{fluid1}} \quad (5)$$

If it is assumed that there is no evaporation of liquid from the wick, the maximum rise of liquid in the wick can be determined by balancing the capillary pressure to the hydrostatic pressure of the liquid in the wick [14]:

$$H = \frac{2\sigma \cos \theta}{gr(\rho_l - \rho_v)} \approx \frac{2\sigma \cos \theta}{gr(\rho_l)} = \frac{2\sigma}{gr_{eff}\rho_l} \quad (6)$$

where the last 2 terms presuppose $\rho_l \gg \rho_v$, which is often justifiable. Eq. (6) can alternatively be used to determine the contact angle if the actual radius, r , and the maximum wetted height, H , are known. The maximum wetted height (i.e. the observed height) may be read visually from a capillary rise experiment by use of a ruler, alternatively the maximum wetted height can be calculated from weight measurements of the amount of liquid wetting the wick, further discussed in the next section. Normally, there will be liquid evaporating from the wick surface, hence there will be flow in the wick even when the maximum height is reached; i.e there is a pressure drop term due to friction in addition to the gravitational pressure term. Assuming uniform evaporation on the wick surface, the pressure balance at the maximum wetted height (steady state condition) requires

$$\Delta p_{cap} + \Delta p_{hs} + \Delta p_{fric} = 0 \quad (7)$$

i.e.

$$\frac{2\sigma}{r_{eff}} = \rho_l g H + \frac{\mu_l}{\kappa \rho_l A_c} \dot{m}_{max} \left(\frac{H}{2} \right) \quad (8)$$

where \dot{m}_{max} is the evaporating liquid mass flow rate. Eq. (8) can be combined with Eq. (4) to yield:

$$\theta = \cos^{-1} \left(\left(\frac{r}{2\sigma} \right) \left(\rho_l g H + \frac{\mu}{\kappa \rho_l A_c} \dot{m}_{max} \left(\frac{H}{2} \right) \right) \right) \quad (9)$$

Eq. (9) is an implicit equation as the maximum evaporating mass flow rate, \dot{m}_{max} , is a function of the permeability, κ , and the effective pore radius, r_{eff} , as seen from Eq. (8), and the effective pore radius is again a function of the contact angle, θ . In order to estimate θ

from Eq. (9) it is thus necessary to have information about the (physical) pore radius, r , the maximum wetted height, H , the permeability, κ , and the evaporating mass flow rate, \dot{m}_{\max} . In the following some methods to determine these parameters are presented and discussed, and calculations are carried out for the nickel foam wicks and using heptane, as a model working fluid.

According to Queheillalt et al. [14] the pore radius, r , of the nickel foam after compression may be estimated from:

$$r = r_0 \frac{\delta}{\delta_0} \quad (10)$$

where r_0 is pore radius of the uncompressed foam and (δ/δ_0) is the thickness ratio.

Eq. (10) was tested experimentally by Queheillalt et al. [14] for wicks of compressed nickel foam together with water. Perfect wetting, i.e. $\cos(\theta)=1$, was assumed. Their predicted equilibrium pumping heights by use of Eq. (6) and Eq. (10) were, interpreted from their data, approximately 25% too high compared to their experimental results with water. They attributed this difference to tortuous pore morphology not being accounted for in the capillary tube model. However, the predicted heights would also have been lower if a contact angle $\theta>0^\circ$ had been assumed instead of perfect wetting ($\theta=0^\circ$).

If the physical radius, r , is determined from Eq. (10) and the effective radius, r_{eff} , is determined by an independent method, such as a rate-of-rise experiment, the contact angle can be estimated from Eq. (11):

$$\theta = \cos^{-1} \left(\frac{r}{r_{\text{eff}}} \right) \quad (11)$$

When the permeability and effective radius are known, the maximum obtainable mass flow rate for a given application can be determined from the pressure balance between the capillary pressure, the hydrostatic pressure, and the frictional pressure. The momentum change of the fluid is small and is therefore disregarded. The resulting maximum heat duty of a particular wick/fluid combination is calculated from

$$\dot{Q} = \dot{m}_{y=0} h_{fg} = \frac{2\kappa A_c \rho}{H \mu} \left(\frac{2\sigma}{r_{\text{eff}}} - \rho g H \right) h_{fg} \quad (12)$$

2.1 Rate-of-rise experiments

The permeability and the effective pore radius may be determined from a rate-of-rise experiment, in which the rate of wetting of an initially dry vertical wick is measured. Historically the rate of rise has been determined by different experimental techniques, usually based on visual detection or mass measurements, and the data analysis in each case depends on the technique applied. In this study the rate-of-rise was derived from measurements of

the total liquid mass uptake, measured as mass loss from a liquid pool. In this way the total mass uptake included both the mass of liquid in the wick and the cumulative mass of liquid evaporating from the wick. Heptane was used as model fluid in the rate-of-rise experiments, since the reactivity of potassium with air and moisture makes rate-of-rise experiments with potassium very complicated. Holley and Faghri [18] derived time-height relationships for rate-of-rise experiments both with and without evaporation of the model fluid from the wick. They, like in this study, measured the mass uptake from a liquid reservoir. In the analysis of their experimental data they assumed no evaporation, as it was most convenient for reducing the data, and thereafter estimated the consequences of evaporation. They derived Equation (13) for the change of mass with time [18].

$$-\left[\frac{2\sigma}{r_{eff}} \ln \left(1 - \frac{g r_{eff}}{2\sigma A_c \varepsilon} m \right) + \frac{g}{A_c \varepsilon} m \right] = \frac{\kappa \rho^2 g^2}{\varepsilon \mu} t \quad (13)$$

All the liquid entering the wick was converted to height, y , by use of Eq. (14). This implied that the calculated wetted height was artificial as it differed from the real observable height (provided that the mass measured is the cumulative total mass uptake from the reservoir, as in this study).

$$y = \frac{m}{\rho A \varepsilon} \quad (14)$$

The error of this approach increases with increasing time and with increasing evaporation rates, i.e. volatile fluids cause larger “evaporation errors” than less volatile fluids. The error due to evaporation is also larger for low permeability wicks [18], as evaporation then takes place over a longer period of time. This is further analysed in the Results and discussion section.

It may take a significant time to reach an absolute maximum height; Fries et al. [19] reported typically 5 days for their systems consisting of stainless steel Dutch twilled weave and different model fluids resembling satellite propellants, all having near zero static contact angle on the weave. For uncompressed nickel foam and water, Huang, Franchi and Cai [16] reported ca. one hour to reach final height, while for their bimodal wicks the front was still moving after about 24 h. In order to limit the experimental time they decided to measure all capillary heights 400 min after immersion. In contrast to this Holley and Faghri [18] used data for typically the first 50-200 s in their rate-of-rise analysis. Fries et al. [19] analysed the time needed to reach 99% of maximum height, and found that this time increased with decreasing evaporation rate. Contrary to this, the error related to ignoring the evaporation in the rate-of-rise analysis increases with increasing evaporation rate and with increasing duration of the experiment.

The working fluid in the rate-of-rise experiments in this study was heptane. A petri dish with heptane was resting on a balance and the wick was hanging from a stand, see Figure 1.

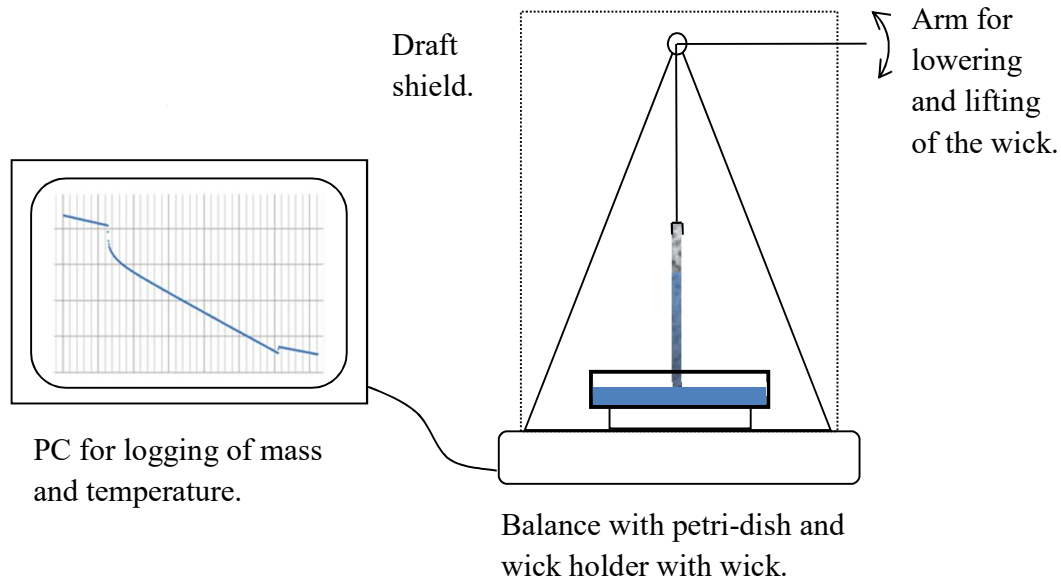


Fig. 1. The rate-of-rise setup.

The rates of rise of heptane in the wicks were calculated from the mass uptake when the lower tips of the wicks were immersed in the heptane. The mass-time data from the balance was recorded with a PC running LabView. Before the wick tip was immersed, the evaporation rate of heptane from the petri dish was determined. Next, the wick tip was immersed and the heptane rose up to the maximum height. At the maximum height there was evaporation of heptane both from the entire wetted surface of the wick as well as from the petri dish. The evaporation rate from the wick was calculated by subtracting the evaporation rate from the petri dish from the total measured evaporation rate from the dish and wick. Constant, uniform evaporation flux was assumed from the wick surface. The temperature of the heptane in the petri dish was measured before the immersion and after the wick was pulled out of the heptane and the thermophysical data for the heptane were determined at the average of these two temperatures.

The analysis of the rate-of-rise data was carried out according to:

1. The height-time data were determined from the measured mass-time data by use of a MatLab-script [20]. The mass-to-height calculations involved subtraction of the evaporated mass from the measured mass-time data and conversion to height by taking the wick cross-sectional area and porosity into account.
2. The rate-of-rise relationship assuming no evaporation, Equation (13), was fitted to the calculated height-time data series. The independent variables were the effective pore radius and the permeability.

The approach did not take into account the evaporating mass flow rate in the determination of the effective pore radius and the permeability, and the calculated effective pore radii and

permeabilities were therefore slightly conservative. Alternatively, a simple conversion of the measured mass data directly to height by use of Eq. (14) would have overestimated the heights compared to the real heights.

3. Wick fabrication

In this study two different nickel foams were used, with the manufacturer's specifications for the uncompressed foams given in Table 1.

Table 1 Manufacturer's data for the uncompressed nickel foams used in this study

| Parameter | Thickness | Pore size | Density |
|-----------|-----------|-------------|----------------------|
| Foam 1 | 1.45 mm | 450 microns | 380 g/m ² |
| Foam 2 | 1.7 mm | 580 microns | 429 g/m ² |

From these foams, 12 two-layer compressed wicks were produced; wicks 1-4 based on Foam 1 and wicks 5-12 based on Foam 2. All wicks had dimensions WxH 25x100mm. Wick no. 12 was considered the final wick in this study, and was therefore analysed most thoroughly.

3.1 Nickel oxide

Nickel foam as delivered from the factory has a "skin" of nickel oxide. The nickel oxide is mechanically harder than pure nickel, and has higher melting point. It was therefore necessary to let the nickel foam go through a reduction process in which the nickel oxide was reduced to pure nickel before the compression process. The oxidized nickel foam was first cut with scissors to pieces of size 25 x 100 mm. The pieces were then reduced in an oven for 60 min at 800°C in an atmosphere consisting of 95% Ar + 5% H₂ gas. The sample pieces were kept in the same atmosphere also during the heat-up period to 800°C and during the subsequent cool-down to room temperature. After this treatment the nickel foam appeared shiny just as pure unoxidized nickel metal. A maximum reduction temperature of 800°C was selected to be in line with the successful thermal cleaning of Queheillalt et al. [14]. Strictly, we have experienced from previous thermogravimetric analyses that the rate of nickel oxide reduction accelerates at about 350°C. We have also experienced from prior heating tests that oxidized nickel foam is mechanically rigid and visually unaffected by heat treatments even above 1000°C.

3.2 Compression

The de-oxidized pieces of nickel foam were compressed by use of a rolling press, model MR100, which was calibrated by use of feeler gauges. During the compression the pieces of nickel foam increased both in length and width, depending on the thickness ratio. As an example, for the thickness ratio of $\frac{\delta}{\delta_0} = 0.16$ the length of an initially 100 mm long sample increased by 7%. The pieces were cut to correct size by use of scissors after the compression.

3.3 The joining pressure requirement

The wicks were made from two compressed nickel foam layers. The two layers were sintered together at 1100°C maximum temperature in a gas atmosphere containing 95% Ar + 5% H₂. The temperature program is shown in Figure 2, here represented by the temperature measured inside the oven during the actual reduction (first peak) and sintering (second peak) in this case for wicks 5-8.

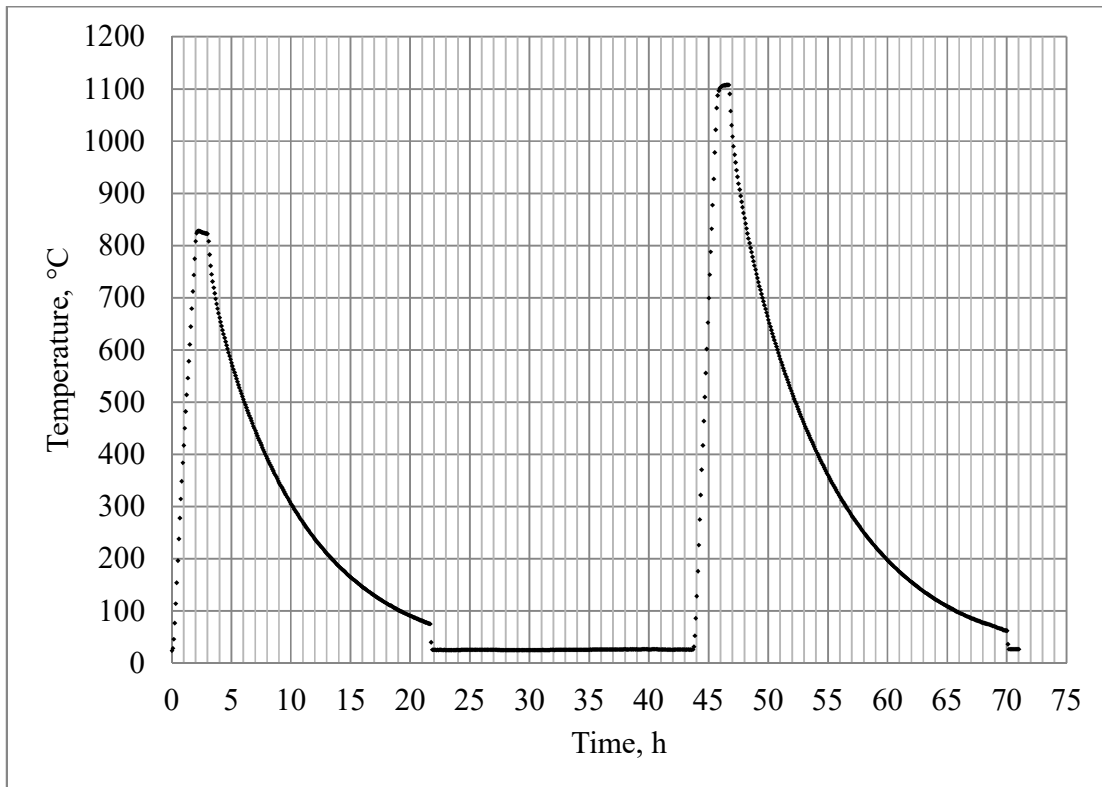


Fig. 2. Measured temperature in oven during reduction and sintering.

During sintering the layers were resting on flat plates of alumina, and alumina plates were also put upon the layers as weights in order to provide contact pressure between the foam layers and avoid buckling. The results from the load pressure requirement study are found in the Results and discussion section.

3.4 Porosity measurements

The porosities were measured for samples cut off wicks 1-8, in addition to samples of uncompressed foam. The porosities were measured using isopropanol, following the procedure described in Ref. [21]. Following this procedure, the porosity was determined from weight measurements of the dry sample, the sample weight submerged in isopropanol and the weight of the sample fully saturated with isopropanol. For wicks 9-12 the porosities were estimated by linear interpolation between the porosities measured for wicks 5 and 6.

3.5 Contact angles with heptane

The contact angles were calculated by use of Eq. (9). Since $\rho_v \ll \rho_l$, the vapour density was disregarded in the calculation. The maximum capillary height was determined from the rate-

of-rise mass data recalculated to heights. As the time required to reach absolute maximum height was in general believed to be very long, the final heights used in these calculations were “quasi-equilibrium” final heights at which the liquid fronts had visually stopped advancing. The pore radius, r , for the different thickness ratios was estimated by use of Eq. (10).

3.6 Wettability

A wettability test using water was carried out using a small piece of nickel foam immediately after the reduction (de-oxidation) process. Spontaneous imbibition occurred. In a similar wettability test performed before the reduction process there was no imbibition, i.e. the untreated nickel foam was hydrophobic. Similarly, in wettability tests carried out about 7, 23 and 48 h after the reduction it was observed that the foam was becoming more and more hydrophobic. After 48 h there was no spontaneous imbibition at all. The observed wettability change from hydrophilic to hydrophobic was likely due to adsorption of volatile organic compounds from the air, as described and analysed for copper metal foams by Shirazy et al. [22]. Similar arguments were used by Sheehan et al. [13] in their study using nickel foam. The observations made in the present work using nickel foam and water were very similar to the results presented by Shirazy et al. [22] using copper foam and water. Even the observed times for the complete wettability transitions in air were similar (48 h). If their theory for copper is transferred to nickel, both the pure nickel surface as well as the oxidized nickel surface are hydrophilic. Following their theory further, the wettability transition from hydrophobic to hydrophilic in the de-oxidation process was caused by desorption of adsorbed organic compounds from the nickel surface, rather than by the removal of oxygen. In a subsequent wettability test a hydrophobic nickel foam sample was rinsed in acetone and then dried for 5 min in air before a new wettability test with distilled water was carried out. It was observed that cleaning with acetone did not make the sample hydrophilic, i.e. cleaning with acetone could not replace the thermal cleaning process.

It should also be noted that heptane, which was used here as test fluid in the rate-of-rise experiments, was always found to wet nickel spontaneously. No analogous experiments were carried out to try to quantify potential changes in the wettability of the nickel-heptane system during the critical 48 h after the reduction process.

The fabrication procedure of the nickel foam wicks is summarized in Figure 3.

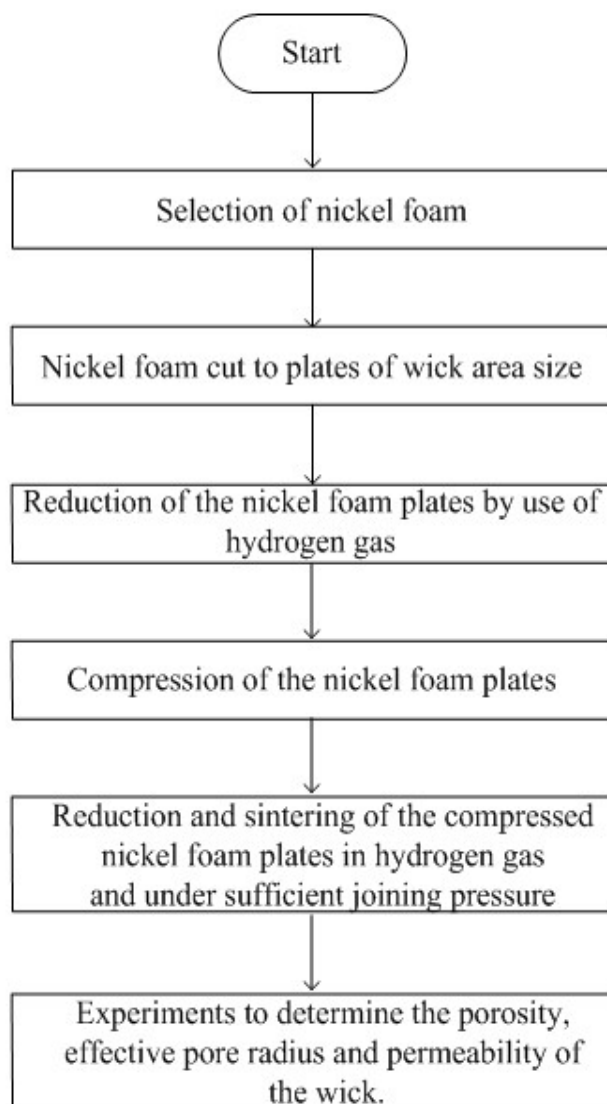


Figure 3. The fabrication process of the nickel foam wicks

4 Results and discussion

4.1 The contact pressure requirement

The compressed nickel foams were sintered together in order to ensure sufficient bonding. By trial and error a contact pressure of 1.2 kPa during sintering was found to give sufficient bonding without affecting the porosity.

4.2 Porosity

The results of the porosity measurements using isopropanol as model fluid are shown in Figure 4.

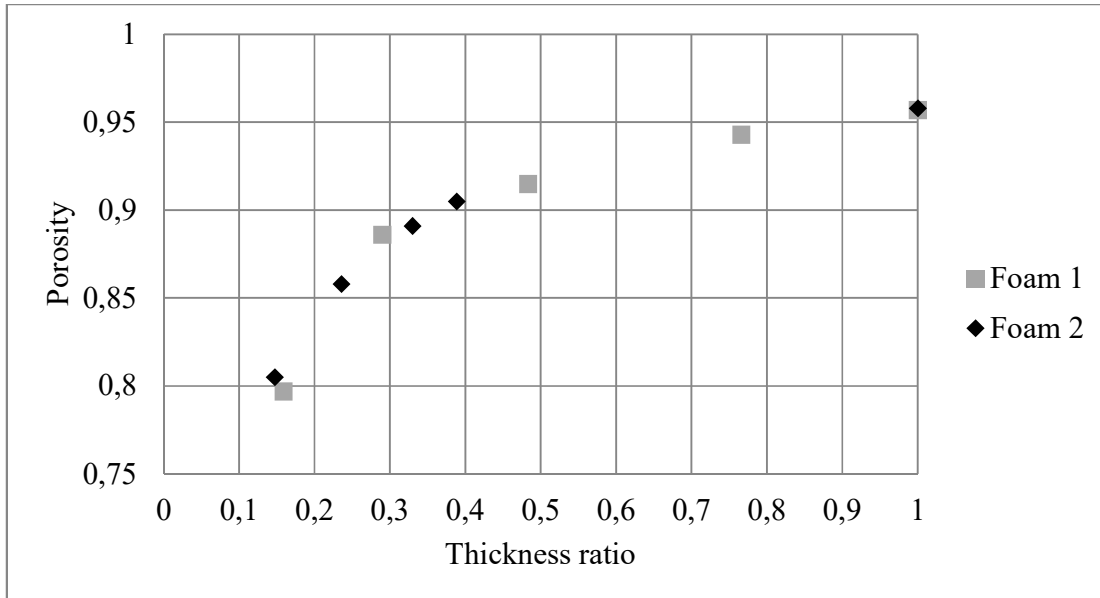


Fig. 4. Measured porosities for wicks of different thickness ratios.

Different contact pressures were applied during the sintering of the wicks made from Foam 1 in the porosity plot, Figure 4, but as long as the different pressures did not cause measurable differences in the thicknesses, the differences in pressures had no impact on the porosities. For the uncompressed foams (thickness ratio = 1) the porosity samples consisted of only 1 layer. From Figure 4 it is observed that the porosity decreases at an increasing rate for decreasing thickness ratio, this is because the volume of the solid material is unchanged while the volume of the void is reduced by the compression. Starting from the porosity of uncompressed foam and assuming 1-D compression, the porosities for different thickness ratios can be predicted approximately. However, such a 1-D model will not be strictly correct because the real compressions also increase the foot-print. Hence, the 1-D theoretical model underpredicts the porosities, and in this study the maximum error was about 11% for the smallest thickness ratio.

4.3 Contact angle

The contact angles for heptane on nickel foam, calculated by Eq. (9) and (10) using data from 4 experiments with Foam 1 wicks and 8 experiments with Foam 2 wicks had an average value of $58.4^\circ \pm 1.3^\circ$ at 95% confidence level [23]. The average temperature of the experiments was 20.7°C . The maximum lifting heights used were the maximum “quasi-equilibrium” heights in the rate-of-rise experiments with heptane, which were carried out 2-4 days after the wicks were sintered. The time period between the sintering and the rate-of-rise experiment is believed to be of less importance when heptane is used than for water, because with heptane there was no observable wettability transition taking place. The maximum “quasi-equilibrium” heights for the different thickness ratios are shown in Figure

5, and were generally higher for wick 1-4 than for wick 5-12 because of the smaller pore size of foam no. 1 than of foam no. 2 (see Table 1).

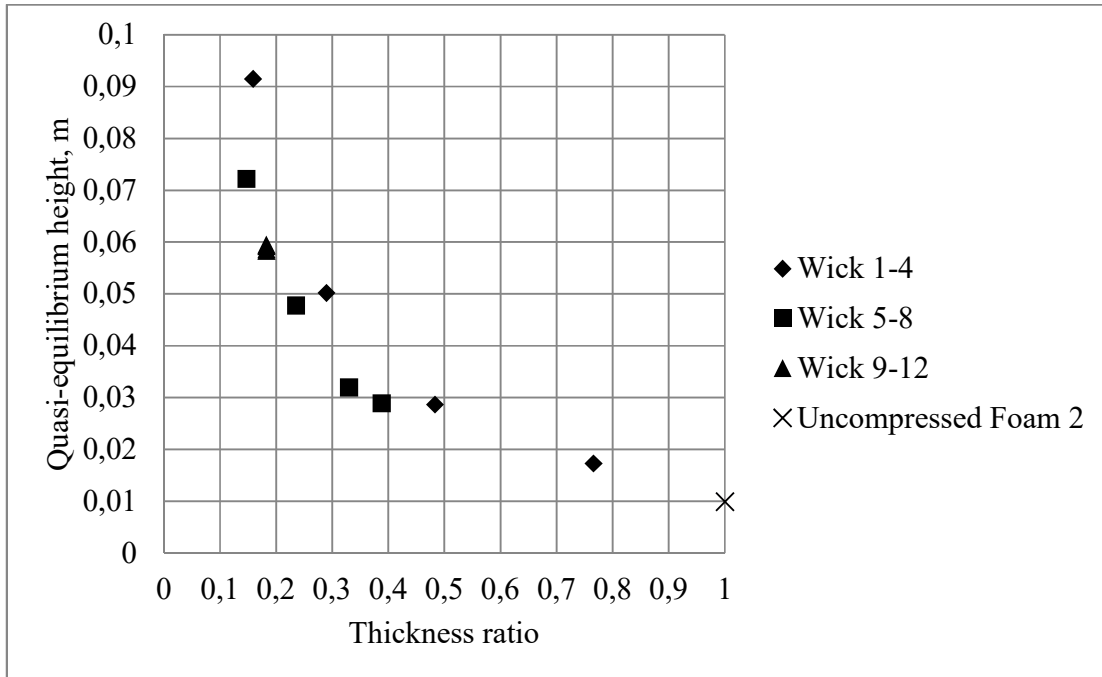


Fig. 5. Quasi-equilibrium maximum heights.

4.4 Rate-of-rise experiments

Figure 6 shows the total mass of heptane imbibing into wick no. 12. The evaporation rate of heptane from the wick is subtracted from the measured weight loss by the balance, yielding the mass remaining in the wick [20]. Figure 7 shows the corresponding wetted heights, where the “calculated observed height” would correspond to an observed height. Figure 8 shows the rate-of-rise calculated from the “calculated observed height”.

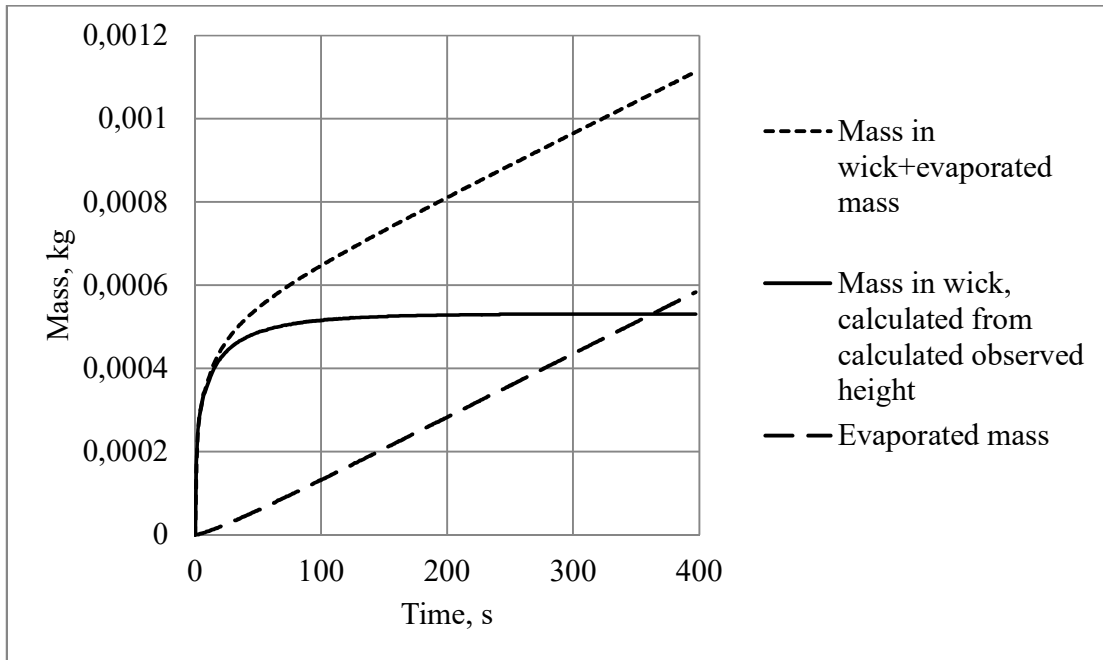


Fig. 6. Masses of heptane during the rate-of-rise experiment for wick 12.

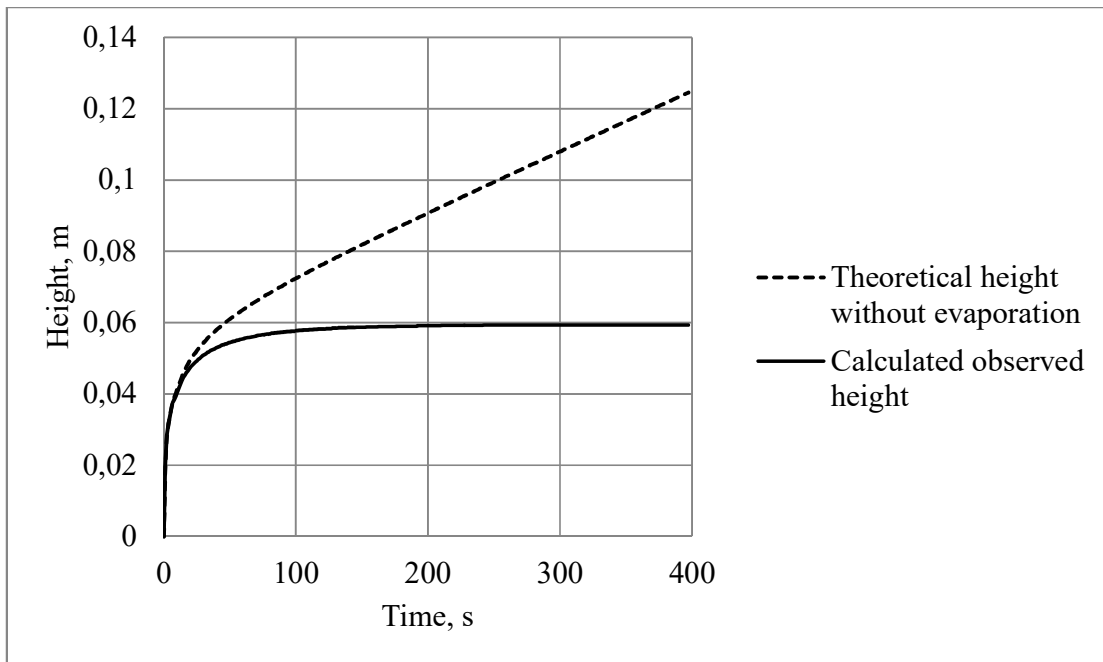


Fig. 7. Heights of heptane in wick 12 during the rate-of-rise experiment.

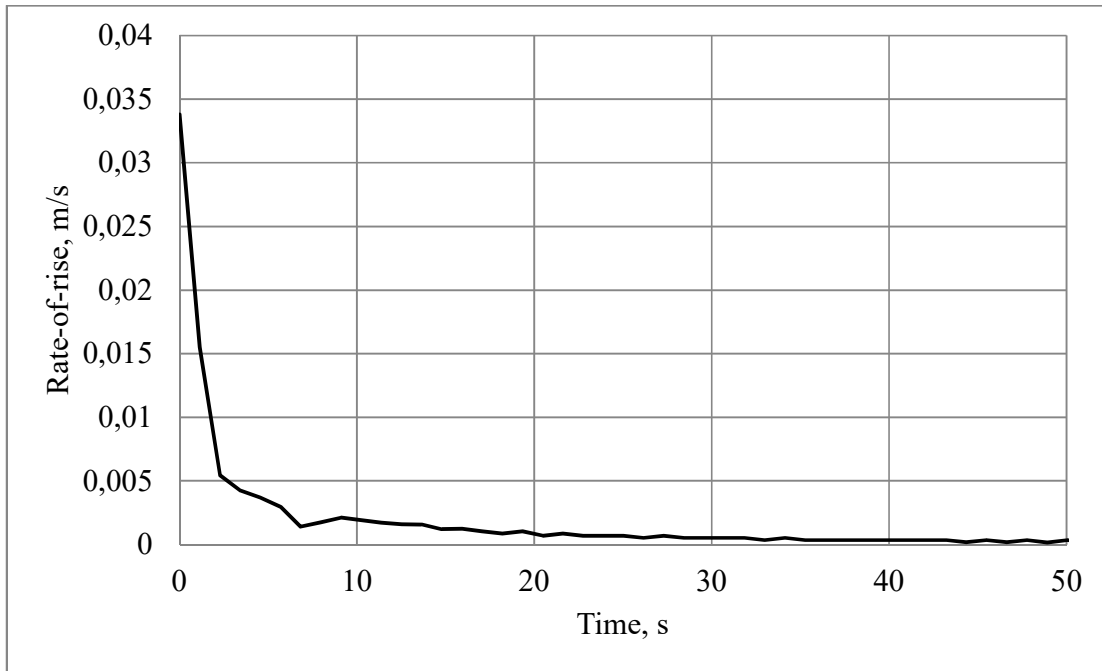


Fig. 8. Rate-of-rise of heptane in wick 12 during the rate-of-rise experiment.

As described previously, the “calculated observed heights” data series was used together with the rate-of-rise theory without evaporation to determine the effective pore radius and permeability. This approach was considered to give slightly conservative estimates (i.e. underestimate the wick capacity) since the frictional pressure drop due to evaporating mass was not taken into account.

If the total mass data series were converted to heights by use of Eq. (14), and the effective pore radius and permeability were determined by use of the theory assuming no evaporation, then it is clear from Figures 6 and 7 that the errors in the effective pore radius and permeability would have increased considerably with time. This was also emphasized by Holley and Faghri [18], who stated that the error due to evaporation would be largest for low permeability wicks. They calculated effective pore radius and permeability assuming no evaporation for experiments which had duration of 50-200 s. They estimated the errors due to evaporation by use of measurements of the evaporation rates from saturated wick samples. In the present work, this error is eliminated by use of the “calculated observed height” dataserries. This approach is, however, not strictly correct, as the mass flow due to evaporation is not taken into account in the calculation of the effective pore radius and the permeability. The magnitude of the error can be deduced from Figure 6 where it is seen that the mass evaporated from the wick constituted a very small part of the total mass uptake during the first seconds of the experiment, after 50 s it constituted about 12%, after 100 s about 25%.

The effective pore radius and permeability for the different thickness ratios are shown in Figure 9 and 10 respectively. Due to the very low equilibrium height ($\approx 10\text{mm}$) and the short duration of the rate-of-rise experiment the uncertainty of the permeability calculation for the uncompressed foam is so high that the value has been omitted from the trendline in Figure 10.

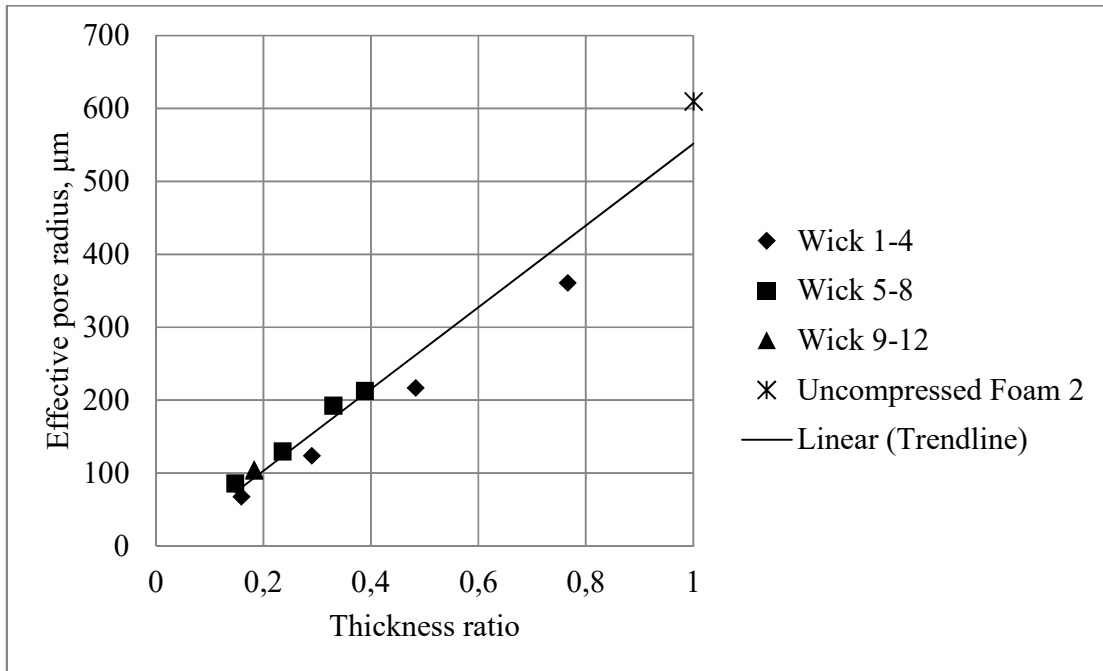


Fig. 9. Effective pore radius.

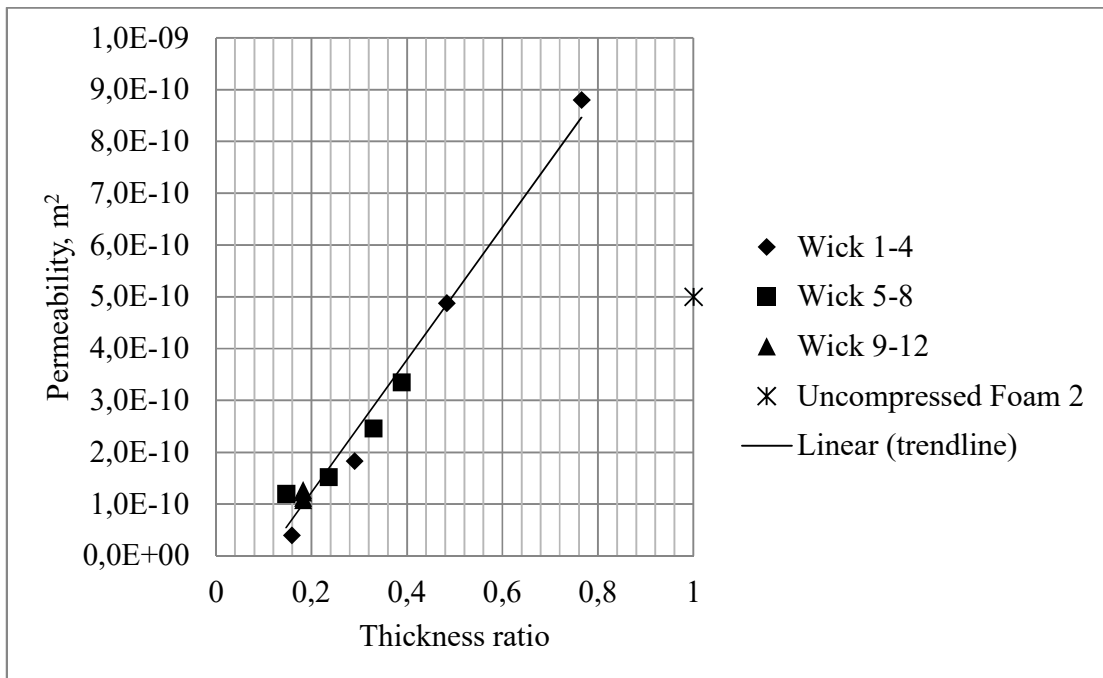


Fig. 10. Permeabilities.

It is unlikely that any heat pipe would require a wick with larger pore size than the pore size of the uncompressed nickel foams, because the capillary pressure would be very low. After considerable compression the nickel foam wicks still had effective pore radii and permeabilities in the upper range, for instance compared to the effective pore radius and

permeability of a “traditional” wick of sintered Inco 255 nickel powder, e.g. $11.9 \mu\text{m}$ and $3.4\mu\text{m}^2$ respectively [18].

4.5 Calculated heat transfer capacity with potassium

In the calculation of the heat transfer capacity using potassium as working fluid the effective pore radius determined from the rate-of-rise experiment with heptane is converted to an effective pore radius for potassium, by use of Eq. (5). From the contact angle calculations performed, a contact angle of 58.4° was used for the heptane on the wick surface. A contact angle of 0° of potassium on the nickel wick surface was assumed [24]. For wick no. 12 at 500°C the heat transfer capacity with potassium was calculated to $950 \cdot 10^3 \text{ W/m}^2$ with the same wetted height (0.0593 m) as for the heptane by use of Eq. (12). Wick 12 was 0.63 mm thick and the evaporation was assumed to take place on one side only.

5. Uncertainty analysis

The uncertainty analysis was carried out according to the procedure presented by Moffat [25].

Each variable has an uncertainty which is known or assumed, and the propagation of these uncertainties to the final results (the contact angle, the permeability, the effective pore radius and the heat transfer capacity) were calculated by varying each variable, one by one, in positive and negative direction. The analysis was carried out for wick 12, but the tabulated uncertainties are considered representative for all wicks as the equations, equipment and experimental approach were similar.

The analysis showed that the uncertainty mainly comes from the wick thickness measurements, made by use of vernier calipers (uncertainty of $\pm 0.03 \text{ mm}$), and the pore radius of the uncompressed foam (assumed uncertainty of $\pm 10\%$). The uncertainty of the measured weight loss contributed negligibly to the overall uncertainty. The permeability is very sensitive to uncertainties in the wick cross-sectional area, and this propagates to the uncertainty of the heat transfer capacity. The consequences of the uncertainties of the thermophysical properties of heptane and the temperature measurements are negligible. For the porosity measurements the uncertainty claimed by the standard [21] is reported.

The significant uncertainties were added by the root of the sum of squares (RSS), and the results are shown in Table 2.

Table 2 Results of the uncertainty analysis

| | Uncertainty estimate | |
|----------------------------------|----------------------|-------------|
| Porosity | $\pm 0.1\%$ | (Known) |
| Effective pore radius, r_{eff} | $\pm 2\%$ | (Estimated) |

| | | |
|-----------------------------------|--------|--------------|
| Contact angle, heptane on wick | ±8.9% | (Calculated) |
| Permeability, κ | ±26% | (Calculated) |
| Heat transfer capacity, \dot{Q} | ±26.7% | (Calculated) |

The uncertainty related to the use of the capillary tube model as a model for the wick structure was not taken into consideration.

6. Conclusions

Wicks for heat pipes have been made from compressed nickel foam. Wick properties are important in the design of heat pipes and are highly dependent on the degree of compression of the wick. Experiments have been carried out in order to determine porosity, effective pore radius, permeability and maximum lifting height for wicks of different degrees of compression. The results are presented graphically.

The nickel foam wicks fabricated in this study have high effective pore radius and high permeability compared to wicks made of sintered nickel powder of type Inco 255. The compressed foam wicks are in the upper range of pore sizes applicable for heat pipes due to the large pore sizes of the nickel foams in uncompressed form.

Experiments have shown that wicks of compressed nickel foam are hydrophilic immediately after the sintering at 1100°C, but turn hydrophobic during 48 h storage in lab air. The wettability transition may be caused by adsorption of organic components from the air as indicated by Sheehan et al. [13] and reported for copper metal foams by Shirazy [22].

The contact angle of model fluid heptane on sintered (reduced) nickel foam wicks was determined to $58.4 \pm 1.3^\circ$, measured 2-4 days after sintering, whereas perfect wetting of 0° was assumed for potassium/nickel.

A pressure of 1.2 kPa can safely be applied to compressed nickel foam layers during sintering at 1100°C, and this will provide a mechanically strong multilayer wick.

Material compatibility makes wicks of compressed nickel foam relevant for heat pipes using potassium as working fluid.

Acknowledgements

The authors would like to thank Elkem and the Research Council of Norway for funding this work. Thanks to Rhodri Bowen and Vale Inco Europe Ltd. for providing nickel foam for wicks 1-4. Dr. Ove Paulsen and engineer Ove Darell at SINTEF have provided valuable technical assistance with the sintering oven.

References

- [1] D.A. Reay, P.A. Kew, P.D. Dunn, Heat pipes, Elsevier, Amsterdam, 2006.
- [2] A. Faghri, Heat pipe science and technology, Taylor & Francis, Washington, D.C., 1995.
- [3] G.P. Peterson, An introduction to heat pipes: modeling, testing, and applications, Wiley, New York, 1994.
- [4] C.C. Silverstein, Design and technology of heat pipes for cooling and heat exchange, Hemisphere Pub. Corp., 1992.
- [5] M. Dillig, J. Leimert, J. Karl, Planar High Temperature Heat Pipes for SOFC/SOEC Stack Applications, Fuel Cells, 14 (2014) 479-488.
- [6] J. Choi, W. Sano, W. Zhang, Y. Yuan, Y. Lee, D.-A. Borca-Tasciuc, Experimental investigation on sintered porous wicks for miniature loop heat pipe applications, Experimental Thermal and Fluid Science, 51 (2013) 271-278.
- [7] X. Yang, Y.Y. Yan, D. Mullen, Recent developments of lightweight, high performance heat pipes, Applied Thermal Engineering, 33–34 (2012) 1-14.
- [8] M.R. Hajmohammadi, M. Rahmani, A. Campo, O. Joneydi Shariatzadeh, Optimal design of unequal heat flux elements for optimized heat transfer inside a rectangular duct, Energy, 68 (2014) 609-616.
- [9] M.R. Hajmohammadi, A. Campo, S.S. Nourazar, A.M. Ostad, Improvement of forced convection cooling due to the attachment of heat sources to a conducting thick plate, Journal of heat transfer, 135 (2013) 124504.
- [10] Y. Li, H.-f. He, Z.-x. Zeng, Evaporation and condensation heat transfer in a heat pipe with a sintered-grooved composite wick, Applied Thermal Engineering, 50 (2013) 342-351.
- [11] L. Jiang, H. Yong, Y. Tang, Y. Li, W. Zhou, L. Jiang, J. Gao, Fabrication and thermal performance of porous crack composite wick flattened heat pipe, Applied Thermal Engineering, 66 (2014) 140-147.
- [12] A.B. Solomon, K. Ramachandran, B.C. Pillai, Thermal performance of a heat pipe with nanoparticles coated wick, Applied Thermal Engineering, 36 (2012) 106-112.
- [13] J. Sheehan, D.T. Queheillalt, P.M. Norris, An evaluation of the wicking characteristics of stochastic open-cell nickel foams, in: 2006 ASME International Mechanical Engineering Congress and Exposition, IMECE2006, November 5, 2006 - November 10, 2006, American Society of Mechanical Engineers, Chicago, IL, United states, 2006.
- [14] D.T. Queheillalt, G. Carbajal, G.P. Peterson, H.N.G. Wadley, A multifunctional heat pipe sandwich panel structure, International Journal of Heat and Mass Transfer, 51 (2008) 312-326.
- [15] E.A. Silk, D. Myre, Fractal Loop Heat Pipe performance testing with a compressed carbon foam wick structure, Applied Thermal Engineering, 59 (2013) 290-297.
- [16] X. Huang, G. Franchi, F. Cai, Characterization of porous bi-modal Ni structures, Journal of porous materials, 16 (2009) 165-173.
- [17] P.C. Hiemenz, Principles of colloid and surface chemistry, Dekker, New York, 1986.
- [18] B. Holley, A. Faghri, Permeability and effective pore radius measurements for heat pipe and fuel cell applications, Applied Thermal Engineering, 26 (2006) 448.
- [19] N. Fries, K. Odic, M. Conrath, M. Dreyer, The effect of evaporation on the wicking of liquids into a metallic weave, Journal of Colloid and Interface Science, 321 (2008) 118-129.

- [20] K. Kristjansson, Unpublished work, NTNU, 2009.
- [21] Dense shaped refractory products -- Determination of bulk density, apparent porosity and true porosity, in, International Organization for Standardization, 1998.
- [22] M.R.S. Shirazy, S. Blais, L.G. Frechette, Mechanism of wettability transition in copper metal foams: From superhydrophilic to hydrophobic, Applied Surface Science, 258 (2012) 6416-6424.
- [23] A.J. Wheeler, A.R. Ganji, Introduction to engineering experimentation, Pearson/Prentice Hall, Upper Saddle River, N.J., 2004.
- [24] M. Barlow, P.J. Planting, Wetting of metal surfaces by liquid alkali metals, Journal Name: Z. Metallk., 60: 719-22 (Sept. 1969).; Other Information: Orig. Receipt Date: 31-DEC-69, (1969) Medium: X.
- [25] R.J. Moffat, Describing the uncertainties in experimental results, Experimental Thermal and Fluid Science, 1 (1988) 3-17.